Photospheric Current Spikes And Their Possible Association With Flares - Results from an HMI Data Driven Model

Michael L. Goodman - NASA Marshall Space Flight Center/Jacobs ESSSA

michael.l.goodman@nasa.gov

Chiman Kwan, Bulent Ayhan & Eric L. Shang - Applied Research, LLC

Work Partially Supported by the NASA SBIR Grant Program

JACOBS
ESSSA Group

Abstract

A data driven, near photospheric magnetohydrodynamic model predicts spikes in the horizontal current density, and associated resistive heating rate per unit volume Q. The spikes appear as increases by orders of magnitude above background values in neutral line regions (NLRs) of active regions (ARs). The largest spikes typically occur a few hours to a few days prior to M or X flares. The spikes correspond to large vertical derivatives of the horizontal magnetic field. The model takes as input the photospheric magnetic field observed by the Helioseismic & Magnetic Imager (HMI) on the Solar Dynamics Observatory (SDO) satellite. This 2.5 D field is used to determine an analytic expression for a 3 D magnetic field, from which the current density, vector potential, and electric field are computed in every AR pixel for 14 ARs. The field is not assumed to be force-free. The spurious 6, 12, and 24 hour Doppler periods due to SDO orbital motion are filtered out of the time series of the HMI magnetic field for each pixel using a band pass filter. The subset of spikes analyzed at the pixel level are found to occur on HMI and granulation scales of 1 arcsec and 12 minutes. Spikes are found in ARs with and without M or X flares, and outside as well as inside NLRs, but the largest spikes are localized in the NLRs of ARs with M or X flares. The energy to drive the heating associated with the largest current spikes comes from bulk flow kinetic energy, not the electromagnetic field, and the current density is highly non-force free. The results suggest that, in combination with the model, HMI is revealing strong, convection driven, non-force free heating events on granulation scales, and that it is plausible these events are correlated with subsequent M or X flares. More and longer time series need to be analyzed to determine if such a correlation exists.

Above an AR dependent threshold value of Q, the number of events $N(Q)$ with heating rates $\geq Q$ obeys a scale invariant power law distribution for each AR given by $N(Q) \propto Q^{-S}$, where $0.40 \leq S \leq 0.53$, with a mean and standard deviation across the 14 ARs of 0.47 and 0.045, showing there is little variation of S from one AR to another. These properties of $N(Q)$ are in close agreement with those of the distribution $N(E)$ for the total energy E of solar flares, determined from observations to be $N(E) =$ constant $\times E^{-\alpha}$. From observations of nanoflares in the $0.7 - 4$ MK range, and from observations of flares in hard X-rays, it is found that $0.51 \leq \alpha \leq 0.57$, and $0.4 \leq \alpha \leq 0.6$, respectively (Crosby et al. 1993, Sol. Phys., 143, 275; Aschwanden & Parnell 2002, ApJ, 572, 1048). Observations also show that, as is found here for the exponent S, there is little variation of α with AR (Wheatland 2000, ApJ, 532, 1209), indicating $N(E)$ and $N(Q)$ are largely independent of individual properties of ARs such as area, total magnetic flux, and distribution of current density (i.e. non-potentiality). Therefore the power law scaling of the *photospheric* heating rate Q computed here on *granulation* scales is essentially identical to that found for *coronal* observations of flare energies on scales 1-2 orders of magnitude larger. This suggests the physical mechanisms that cause Q and coronal flares are closely related. It seems likely that Q is the signature of a magnetic reconnection process

in an energy range and volume orders of magnitude smaller than those of flares. In this context, at least the larger spikes in Q might be signatures of UV photospheric or lower chromospheric bombs in which plasma is heated to temperatures $\sim 10^5$ K (Peter et al. 2014, Science 346, 1255726; Judge 2015, ApJ, 808, 116). In addition, lattice based avalanche simulations of flare energy release predict $0.4 \leq \alpha \leq 0.5$, while analytic, fractal-diffusive self organized criticality models predict $0.4 \leq \alpha \leq 0.67$, in excellent agreement with observations, and the results presented here (Aschwanden & Parnell 2002, ApJ, 572, 1048; Aschwanden 2012, A&A, 539, A2; Aschwanden 2013, in "Self Organized Criticality Systems"; Aschwanden et al. 2016, SSR, 198, 47).

Questions:

- **Are there changes in the photospheric current density J in NLRs of ARs that are useful for forecasting M/X flares?**
- **Can HMI (Helioseismic & Magnetic Imager) be used to detect previously undetected changes in J distribution?**

Approach:

- **HMI: Full disk, continuous time observations of photospheric B at $1''$, 12 minute resolution. High enough to begin to resolve granulation dynamics: space and time scales ~ 1000 km and $\sim 15 - 20$ minutes.**
- **Use HMI time series of the 2D $\mathbf{B}(x, y, t)$ to determine an analytic model for the 3D $\mathbf{B}(x, y, z, t)$ near the photosphere. Compute $\mathbf{J}, \mathbf{A}, \mathbf{E}$ in each pixel for 14 ARs. 7 with M/X flares. 7 with B, C, or no flares.**
- **Compute time series of $Q(t) = \eta J^2$ (+ other quantities) for each AR NLR(t). Are there correlations with M/X flare occurrence times?**

  Answer: Plausibly yes, but need to analyze more ARs for good statistics.
- **Compute the cumulative distribution function (CDF) $N(Q)$ for each AR time series of Q. $N(Q)$ is the number of events with heating rates $\geq Q$. Compare with the observed $N(E)$ for the total energy E of solar flares.**

  Result: $N(Q)$ is found to be a scale invariant power law distribution, like $N(E)$, and to have essentially the same exponent range, suggesting a common cause for the *photospheric* heating events found here on *granulation* scales, and the large *coronal* heating events (flares) on spatial scales $10 - 100$ times larger.

1. Magnetic Field Model

$$\mathbf{B}(x,y,z,t) = e^{-z/L(x,y,t)} \sum_{n=0}^{N_x} \sum_{m=0}^{N_y} \mathbf{b}_{nm}(t) e^{2\pi i \left(\frac{nx}{L_x} + \frac{my}{L_y}\right)}. \quad (1)$$

$L(x,y,t) = L_0(x,y,t) + zL_1(x,y,t)/L_0$, determined by the HMI data and the $\nabla \cdot \mathbf{B} = 0$ condition. No force-free assumption. Need full J. A 2D $\mathbf{B}(x,y,t)$ only gives J_z.

2. Vector Potential, Electric Field, Ohm's Law

Solve $\mathbf{A} = \nabla \times \mathbf{B}, \nabla \cdot \mathbf{A} = 0$ analytically.

$$\mathbf{E} = -\frac{1}{c}\frac{\partial \mathbf{A}}{\partial t} - \nabla\phi \sim -\frac{1}{c}\frac{\partial \mathbf{A}}{\partial t}. \quad (2)$$

Ohm's law: $\mathbf{E} + (\mathbf{V} \times \mathbf{B})/c = \eta \mathbf{J}$. $\eta = 2 \times 10^{-12}$ sec.

3. Solution Steps

The 12 minute averaged data from the hmi.sharp_720s_cea data series are used to minimize effects of noise. Every 12 minutes HMI provides a full disk map of B.

- **Filter out the 6, 12, and 24 hour periods in the time series of $\mathbf{B}_{HMI}$ for each pixel using a bandpass filter. Corrects for spurious Doppler periods induced by SDO orbital motion.**
- **Set $\mathbf{B}(x,y,0,t) = \mathbf{B}_{HMI}(x,y,t)$. Use FFT to solve for the $\mathbf{b}_{nm}(t)$ in Eq. (1).**
- **Set $\nabla \cdot \mathbf{B}(x,y,z,t) = 0$. Expand through order z. Solve for $L_0(x,y,t)$ and $L_1(x,y,t)$. B is divergence free through order z.**
- **Determine the NLR(t) of each AR using Schrijver's algorithm (2007, ApJ).**
- **At each time, compute the pixel, and the NLR integrated values of $Q, \mathbf{J} \cdot \mathbf{E}$, and $R_{CM} \equiv \mathbf{V} \cdot (\mathbf{J} \times \mathbf{B})/c$.**
  $\mathbf{J} \cdot \mathbf{E} = Q + R_{CM}$ (EM, CM KE, and thermal energy balance).
  Convection driven heating dominates if $Q \sim -R_{CM}$ (i.e. $|\mathbf{J} \cdot \mathbf{E}|/Q \ll 1$).
- **Compute power spectra, spectrograms, and CDFs of the time series of Q for each AR.**

4. Removal of Spurious Doppler Periods From the HMI B

There is spurious, Doppler shift generated noise in the form of 6, 12, and 24 hour period oscillations in the components of B for each pixel, corresponding to frequencies of $(4.6296, 2.3148, 1.1574) \times 10^{-5}$ Hz. It causes a slow change in B relative to the granule turnover time since the oscillation periods correspond to $\sim 20 - 90$ turnover times. The Doppler generated noise is significant, as shown in this section. This noise is removed from the time series of HMI B for each pixel using an FFT based bandpass filter. Two versions of the filter were tested. One removes frequencies in an interval of length 0.4166×10^{-5} Hz centered on each of the three noise frequencies. The second version removes the entire frequency range corresponding to the entire 6-24 hour period range. The results of these two filtering methods are found to be essentially identical. This is due to the dominance of the 6, 12, and 24 hour period signals in the 6-24 hour period range. Only results for the first version of the filter are presented here.

Denote the filtered and un-filtered time series for B_x as B_{xf} and B_{xu}, and similarly for other quantities. Figure 1 shows the filtered and un-filtered HMI time series of B_x, B_y, and B_z, the difference between the un-filtered and filtered time series, and the magnitude of their ratio for a randomly selected pixel from the NLR of NOAA AR 1166 during a 70 hour long time series. This AR is one of the SF (=strongly flaring - M and/or X flares) ARs analyzed here. The figure shows that the difference between the filtered and un-filtered time series of B is significant, showing that the Doppler noise can be significant at the single pixel level.

The Doppler noise can also be significant in quantities that are integrals of pixel level quantities over NLRs. For example, again consider the time series for NOAA AR 1166 used for Figure 1. Figures 2-3 show the results of integrating the filtered and un-filtered pixel level results for ηJ^2 and $B^2/8\pi$ over the NLR at each time. The 70 hour long time interval includes 1 X, 2 M, and 9 C flares. For these and subsequent figures, the red, green, and light blue vertical lines and their labels indicate the times and magnitudes of X, M, and C flares. During the 70 hour time interval the number of pixels in the NLR varies across the range of $\sim 3 - 6 \times 10^4$. The figures show that the superposition of un-filtered quantities from each pixel causes a large error in the result.

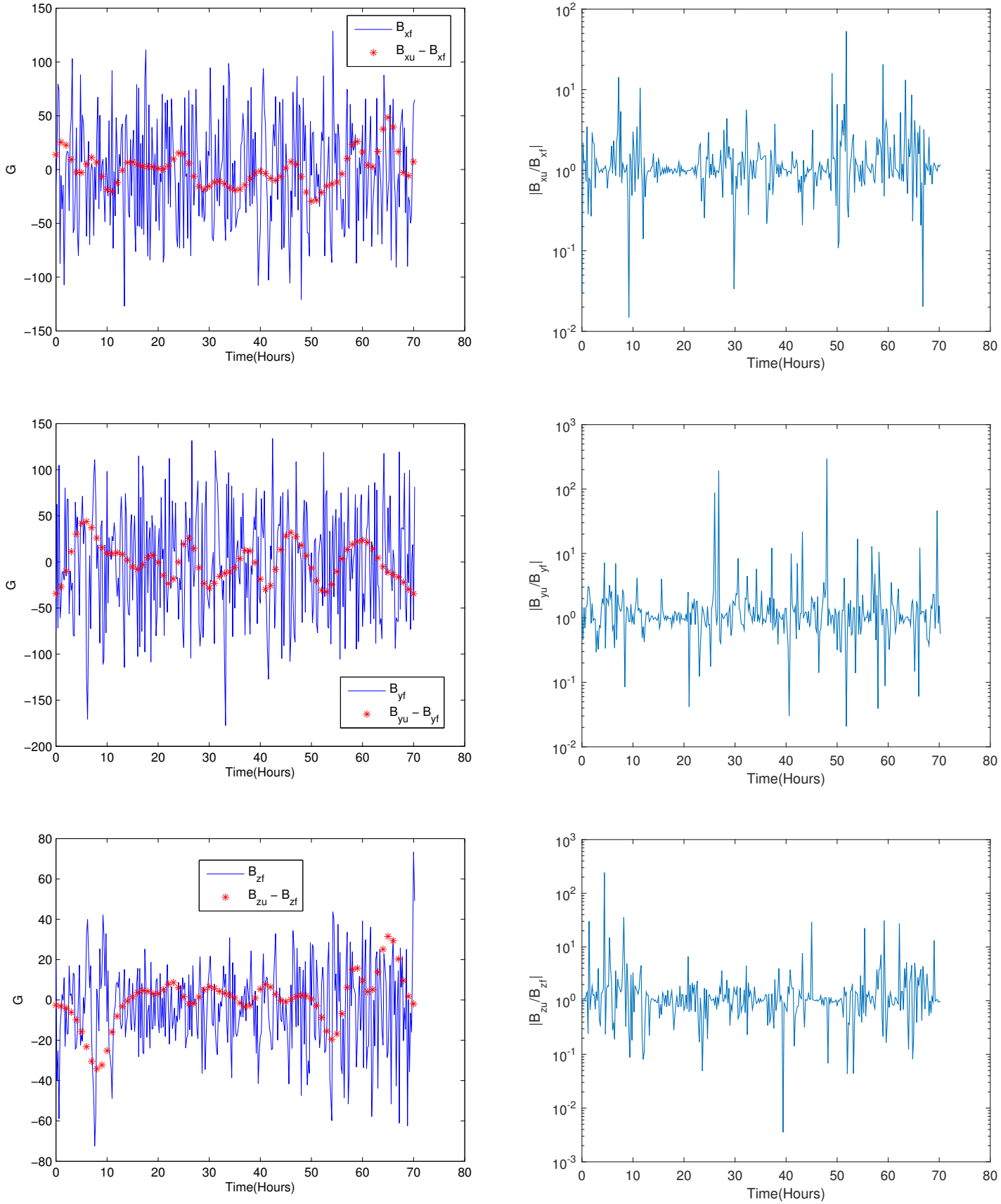

Figure 1: Top, Middle, Bottom: Comparison of the Filtered and Un-filtered B_x, B_y, B_z in a pixel randomly selected from the NLR of AR 1166.

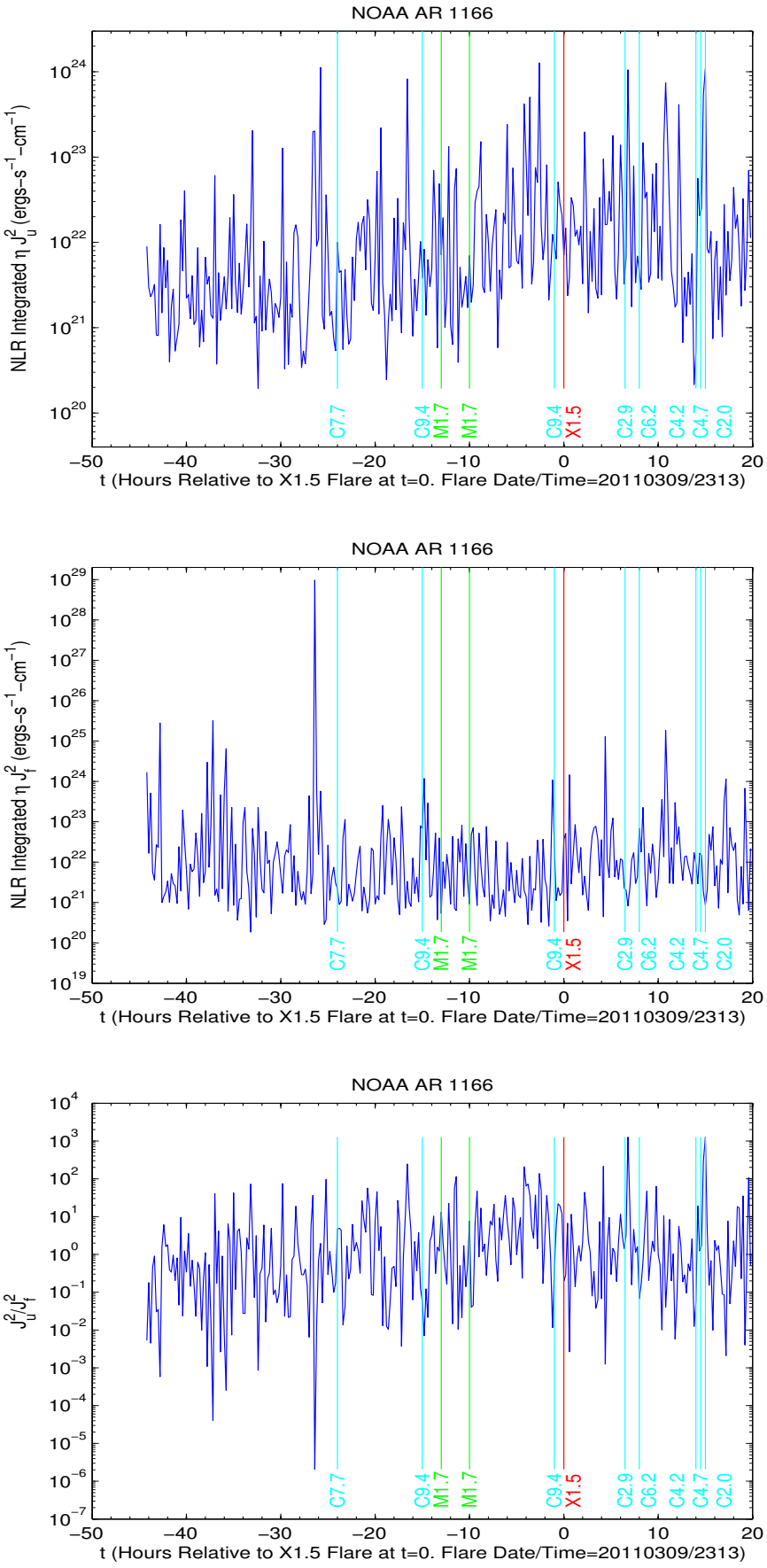

Figure 2: Comparison of the filtered and un-filtered, NLR integrated ηJ^2.

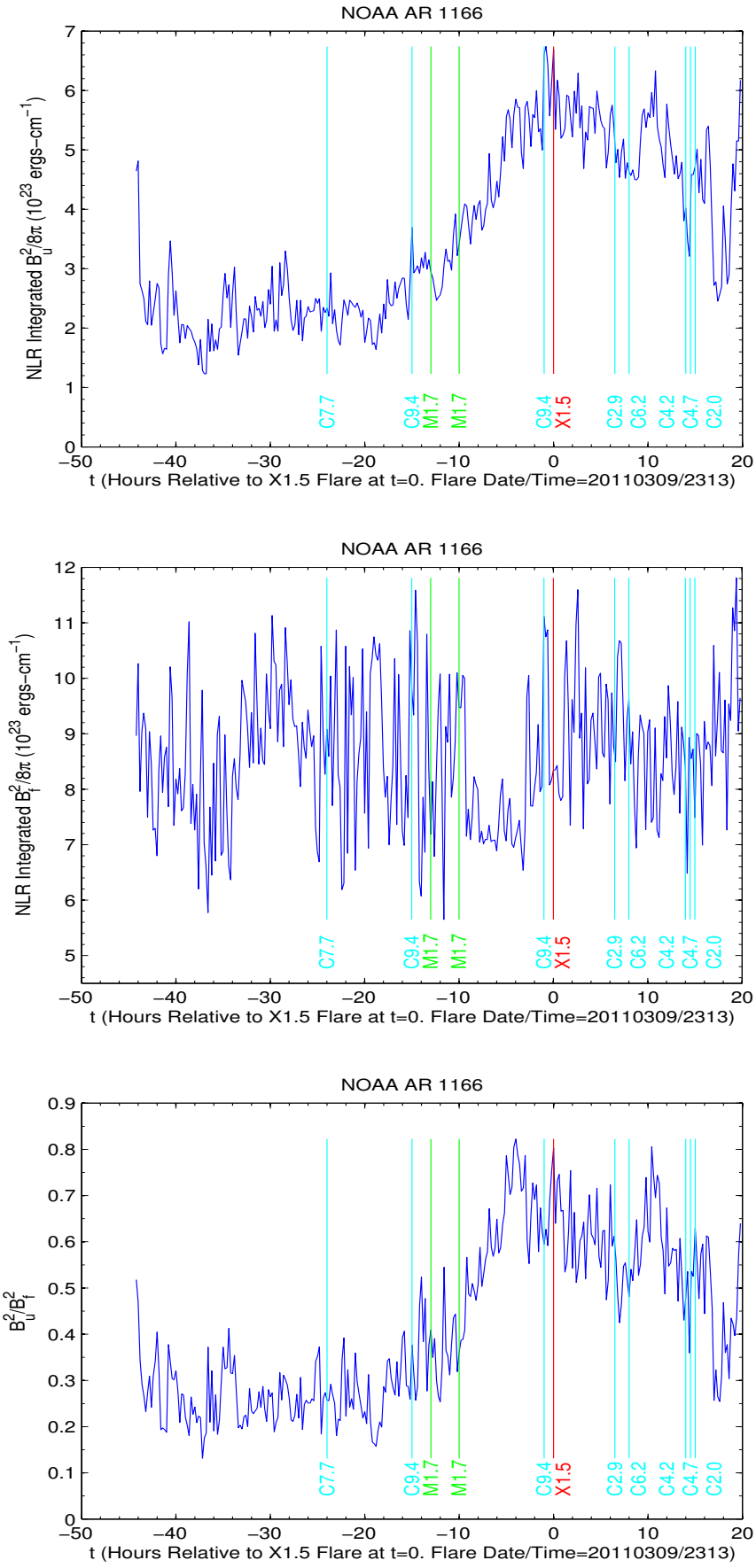

Figure 3: Comparison of the filtered and un-filtered, NLR integrated $B^2/8\pi$.

5. NLR Integrated Resistive Heating Rates Q of Strongly Flaring and Control ARs: Comparison of Heating Spike Times with Subsequent Flaring Times

- **Strongly flaring (SF) ARs are those with M/X flares. Control ARs are those with C, B, or no flares.**

- **Figure 4 and the upper left plot in Figure 5 show the time series of the NLR integrated Q for the 7 SF ARs, and the times of C, M, and X flares.**

  AR 1158: The largest spike by a factor ~ 25 occurs $\sim 38 - 68$ hours before the X and M flares.

  AR 1166: The largest spike is ~ 3.5 orders of magnitude larger than all others, and occurs 26 hours before the X flare. The next 2 largest spikes occur $\sim 38 - 44$ hours before the X flare.

  AR 1261: The 6 largest spikes occur $\sim 18 - 39$ hours before the M flare, and all but one are more than an order of magnitude larger than the 7th largest spike.

  AR 1283: The 3 largest spikes occur $\sim 22 - 25$ hours before the X flare, and the 2 largest of these are more than an order of magnitude larger than the 4th largest spike.

  ARs 1429 and 1430: Magnetically coupled in the sense that they are merging during the time sequence. The 9 largest values of Q occur about one day before the two X flares near t=0, but after the X1.1 flare.

  AR 1890: For values above background values, which are $\lesssim 10^{23}$, Q increases from the left towards the first X1.1 flare, attains its largest value between the two X1.1 flares, and tends to decrease after the second X1.1 flare.

  AR 2017: The largest spike by an order of magnitude occurs ~ 4 hours before the X flare, and the next 2 largest spikes occur $\sim 90 - 105$ hours before the X flare.

  These plots suggest it is plausible that the largest values of Q are correlated with the subsequent occurrence of X and M flares. However, the sample size of 14 ARs is too small to make it clear if such a correlation exists. A study using more and longer time series is needed to determine this.

- **Figures 5-6 show the time series of the NLR integrated R_{CM} for the 7 SF ARs. The plots include the values of Q and $\mathbf{J}\cdot\mathbf{E}$ when Q exceeds a threshold for each time series. Each threshold is the approximate value below which most values of Q occur, and above which the relatively few large spikes occur. The time series show that for values of Q above the threshold, which is almost the same for all 7 SF AR time series ($\sim 10^{22} - 10^{23}$ ergs-cm^{-1}-s^{-1}), Q is very close to $-R_{CM}$. This is the case of convection driven heating: the largest heating events, corresponding to the largest current spikes, are due to the conversion of bulk flow kinetic energy into thermal energy, rather than due to the conversion of magnetic energy into thermal**

energy. This suggests the existence of large heating events in the NLRs of AR photospheres that are convection driven, involving little exchange of energy between the magnetic field and particles, at least during the main phase of thermal energy generation.

Possible reconnection process: Magnetic Energy $\stackrel{RX}{\longrightarrow}$ Bulk Flow Kinetic Energy $\longrightarrow$ Thermal Energy Q. Here $Q \sim -R_{CM} = \mathbf{J}\cdot(\mathbf{V}\times\mathbf{B})/c \equiv \mathbf{J}\cdot\mathbf{E}_{convection}$.

The magnetic field mediates the conversion of bulk flow kinetic energy to thermal energy through the action of the convection electric field.

- **Figures 7-8 shows plots of R_{CM} for 6 of 7 C ARs. The plots include the values of Q and $\mathbf{J}\cdot\mathbf{E}$ when Q exceeds a threshold, chosen in the same way as for Figures 5-6. Similar to the SF ARs, the larger heating rates are convection driven, and the threshold above which convection driven heating dominates is about the same for all ARs ($\sim 10^{21} - 10^{22}$ ergs-cm^{-1}-s^{-1}). Comparing the values of Q in Figures 7-8 with those in Figures 5-6 shows that the larger SF AR Q values are $\sim 10 - 10^3$ times larger than the larger of the C AR Q values.**

  The plots suggest that a correlation of the larger heating events with B and C flares is less likely than for M and X flares.

- **The Largest Heating Events are Highly Non-Force-Free:**

  Let $J_\perp$ and $J_\parallel$ be the current densities perpendicular and parallel to B. Plots of $J_\perp$ and $J_\parallel$, not included here, for the 14 ARs analyzed show that for SF and C ARs the largest current enhancements are due to enhancements in $J_\perp$, which tend to be orders of magnitude larger than $J_\parallel$. Even during flaring sequences with M or X flares, $J_\parallel$ varies by no more than a factor ~ 2, while $J_\perp$ varies by orders of magnitude. This indicates that the largest spikes in Q are due to resistive dissipation of highly non-force-free currents.

  The resulting Lorentz force $(\mathbf{J}\times\mathbf{B})/c$ is found to be essentially downward towards the photosphere.

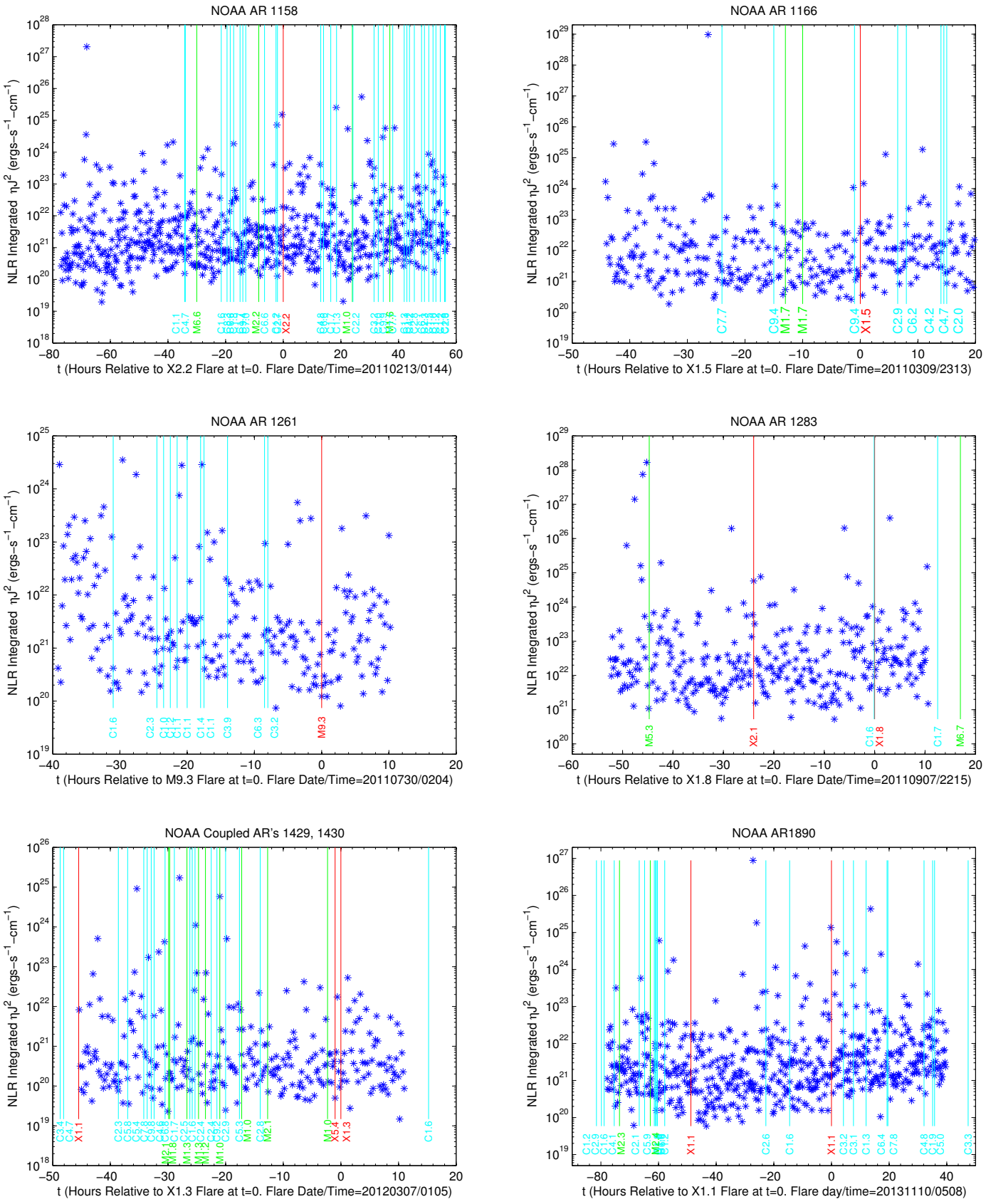

Figure 4: NLR integrated Q for 6 of 7 SF ARs.

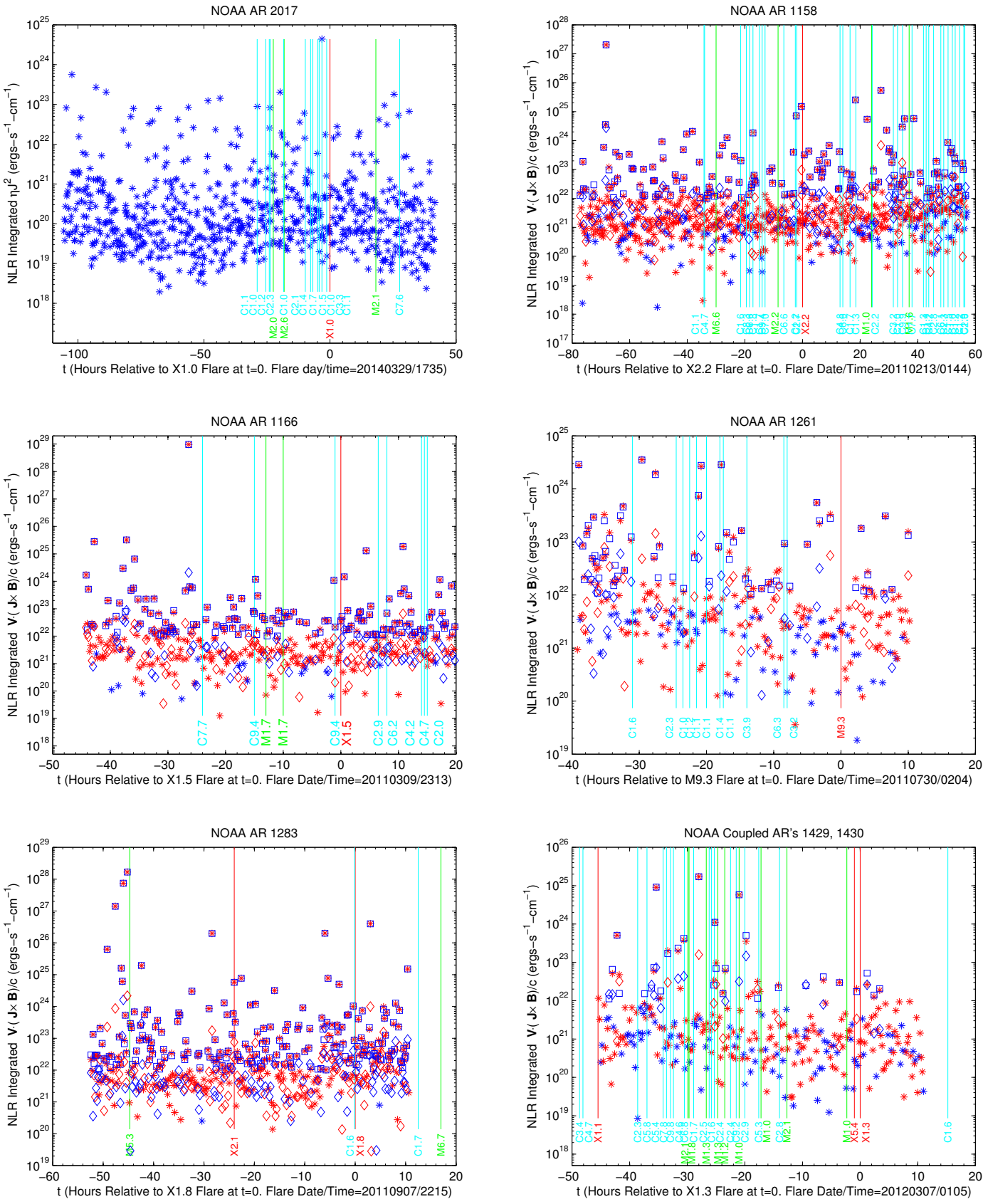

Figure 5: NLR integrated Q for the 7th SF AR, and R_{CM} for 5 of 7 SF ARs. Stars, Squares, Diamonds label values of RCM, Q, and $\mathbf{J} \cdot \mathbf{E}$. Blue/Red indicates positive/negative values. Q and $\mathbf{J} \cdot \mathbf{E}$ are plotted with RCM when the integrated $Q \geq 10^{22}$ ergs-cm^{-1}-s^{-1}.

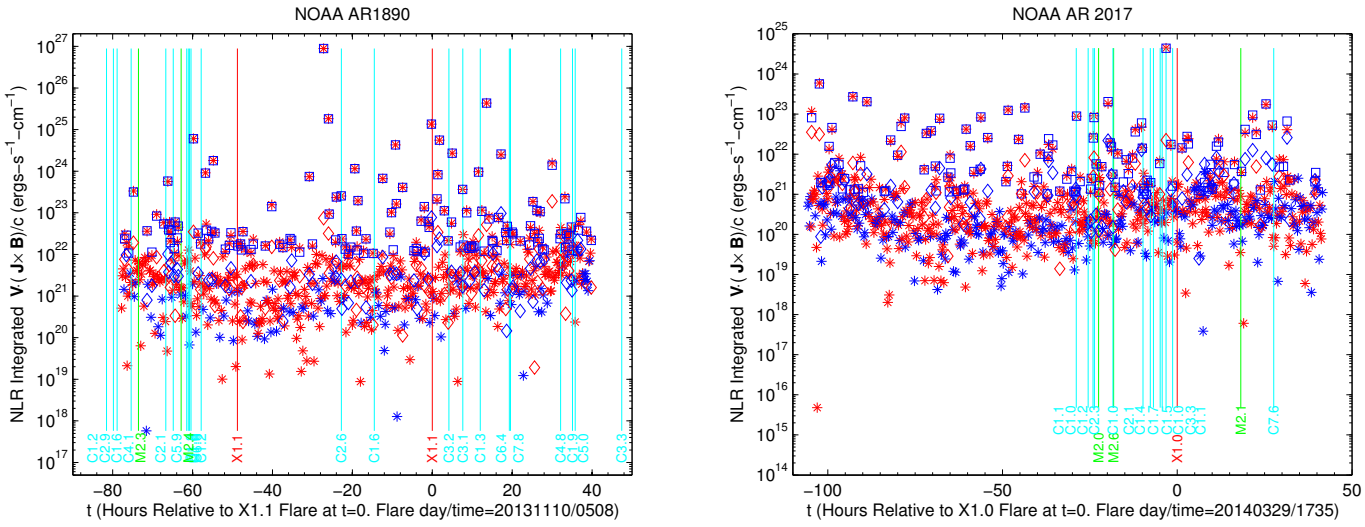

Figure 6: NLR integrated R_{CM} for the remaining 2 of 7 SF ARs. Stars, Squares, Diamonds label values of R_{CM}, Q, and $\mathbf{J} \cdot \mathbf{E}$. Blue/Red indicates positive/negative values. Q and $\mathbf{J} \cdot \mathbf{E}$ are plotted when the integral of $Q \geq 10^{22}(10^{21})$ ergs-cm^{-1}-s^{-1} for the left(right) plot.

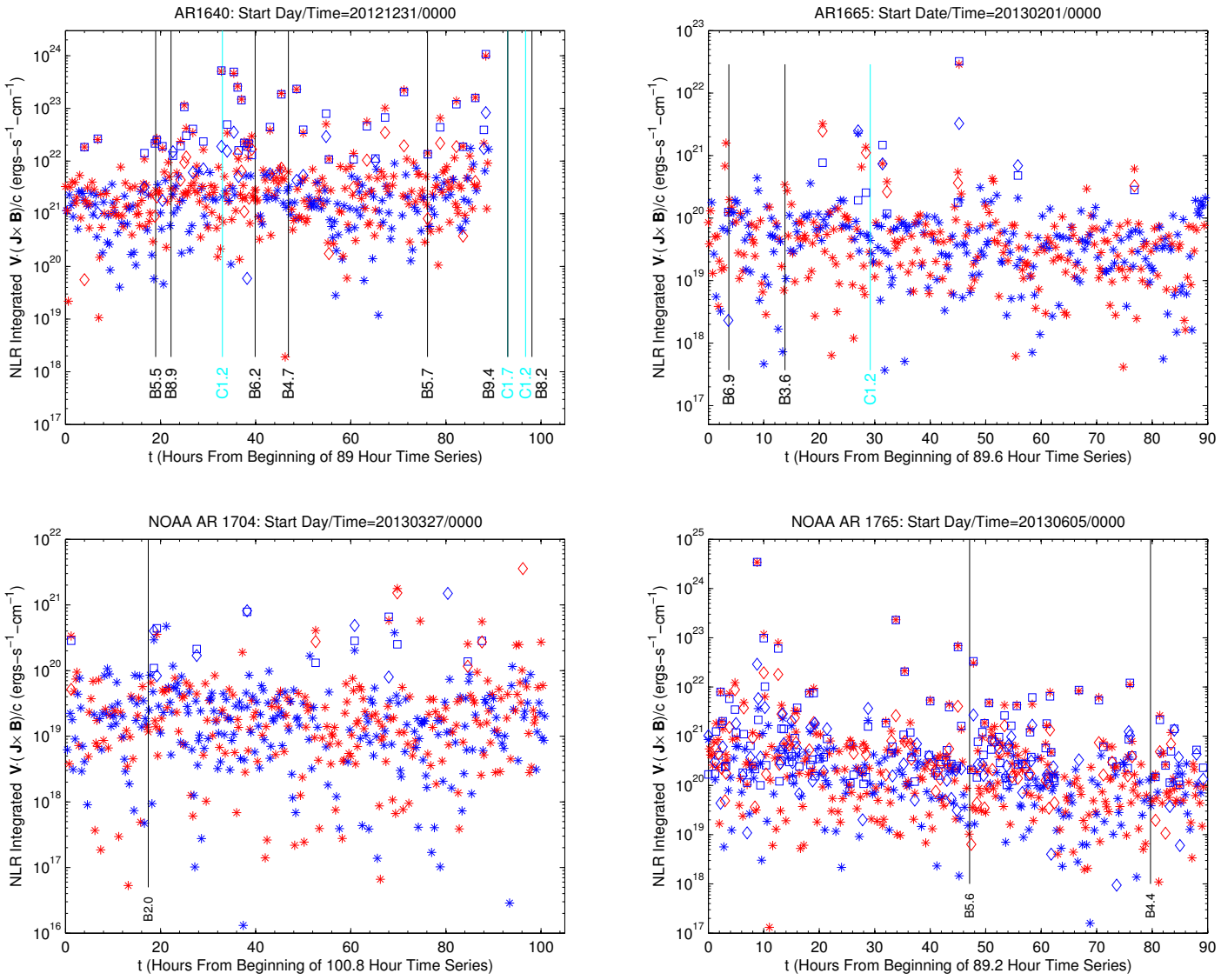

Figure 7: NLR integrated R_{CM} for 4 of 7 C ARs. Stars, Squares, Diamonds label values of R_{CM}, Q, and $\mathbf{J} \cdot \mathbf{E}$. Blue/Red indicates positive/negative values. Q and $\mathbf{J} \cdot \mathbf{E}$ are plotted when the integral of $Q \geq 10^{20}$ and 10^{22} ergs-cm^{-1}-s^{-1} for ARs 1665 and 1640, respectively, and when the integral of $Q \geq 10^{20}$ ergs-cm^{-1}-s^{-1} for ARs 1704 and 1765.

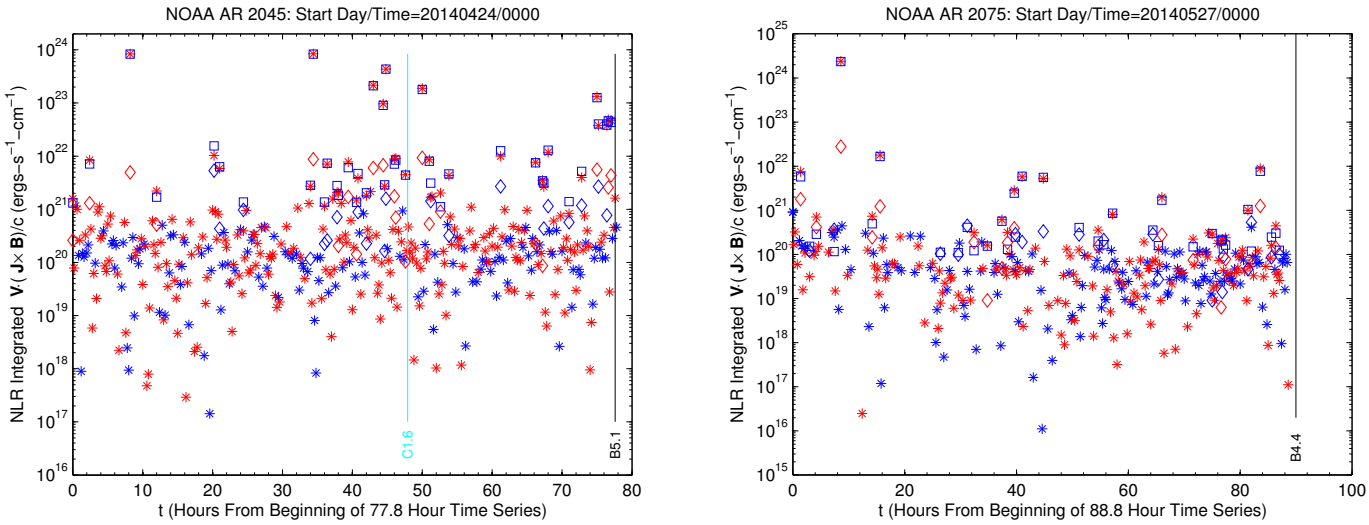

Figure 8: NLR integrated R_{CM} for 2 of 7 C ARs. Stars, Squares, Diamonds label values of R_{CM}, Q, and $\mathbf{J} \cdot \mathbf{E}$. Blue/Red indicates positive/negative values. Q and $\mathbf{J} \cdot \mathbf{E}$ are plotted when the integral of $Q \geq 10^{20}$ and 10^{21} ergs-cm^{-1}-s^{-1} for ARs 2075 and 2045.

6. Are Spikes in Q Signatures of Current Sheet Heating and Photospheric/Chromospheric Bombs?

- **The 3 largest spikes in Q for each AR occur in single pixels, and so occur in areas $\lesssim (0.5'')^2$, and during time intervals $\lesssim 12$ minutes.**
- **In these pixels, J and B are essentially horizontal and $\perp$. This suggests a horizontal current sheet configuration.**
- **The characteristic height H over which $B_{horizontal}$ varies to generate the current spikes should be small. The estimate $H \sim cB/(4\pi J_\perp)$ for the largest spike in each AR gives $H \sim$ cm's - km's.**
- **This suggests that at least the largest spikes are signatures of heating in horizontal, vertically thin current sheets over granulation scale areas.**
- **These spikes might be signatures of photospheric or lower chromospheric bombs seen in IRIS (Interface Region Imaging Spectrograph) UV observations (Peter et. al 2014, Science; Judge 2015, ApJ). The bombs are plasma heated from ~ 6000 to $\sim 10^5$ K, fully ionized for ~ 5 minutes, on spatial scales < 2000 km (granulation space and time scales).**

7. Scale Invariant Power Law Distributions of Q - Comparison with Flares

- **Figures 9-12 show the Cumulative Distribution Functions (CDFs) of the time series for Q. The CDF is the number $N(Q)$ of heating events with heating rate $\geq Q$.**

- **The figures show that above an AR dependent threshold value, the CDF for each AR is well fit by a scale invariant power law distribution of the form $N(Q) = AQ^{-S}$, with S constant over a range of several orders of magnitude in Q.**

  Scale invariance means that a change in scale of Q (i.e. replacing Q by kQ) does not change the form of $N(Q)$ (i.e. $N(kQ) =$ constant $\times N(Q)$). $N(Q)$ is scale invariant over the range of Q for which S is constant.

- **For the 14 ARs it is found that $0.40 \leq S \leq 0.53$, with a mean and standard deviation across the 14 ARs of 0.47 and 0.045, showing there is little variation of S from one AR to another.**

- **The CDF $N(E)$ for the total energy E of solar flares is determined from observations to have the same form: $N(E) =$ constant $\times E^{-\alpha}$.**

- **EUV and SXR observations of nanoflares in the $0.7 - 4$ MK range, and HXR observations of flares imply that $0.51 \leq \alpha \leq 0.57$, and $0.4 \leq \alpha \leq 0.6$, respectively (Aschwanden & Parnell 2002, ApJ, 572, 1048).**

- **Observations also show that, as is found here for the exponent S, there is little variation of α among ARs (Wheatland 2000, ApJ, 532, 1209).**

- **Therefore, the power law scaling of the *photospheric* spikes in Q computed here on *granulation* scales is essentially identical to that found for *coronal* observations of flare energies on scales 1-2 orders of magnitude larger.**

- **This suggests the physical mechanism that causes the photospheric granulation scale heating spikes found here, and coronal flares are closely related.**

- **In addition, lattice based avalanche simulations of flare energy release predict $0.4 \leq \alpha \leq 0.5$, while analytic, fractal-diffusive self organized criticality models predict $0.4 \leq \alpha \leq 0.67$, in excellent agreement with observations, and with the results presented here (Aschwanden & Parnell 2002, ApJ, 572, 1048; Aschwanden 2012, A&A, 539, A2; Aschwanden 2013, in "Self Organized Criticality Systems", M. Aschwanden (Ed.); Aschwanden et al. 2016, Space Sci. Rev. 198, 47).**

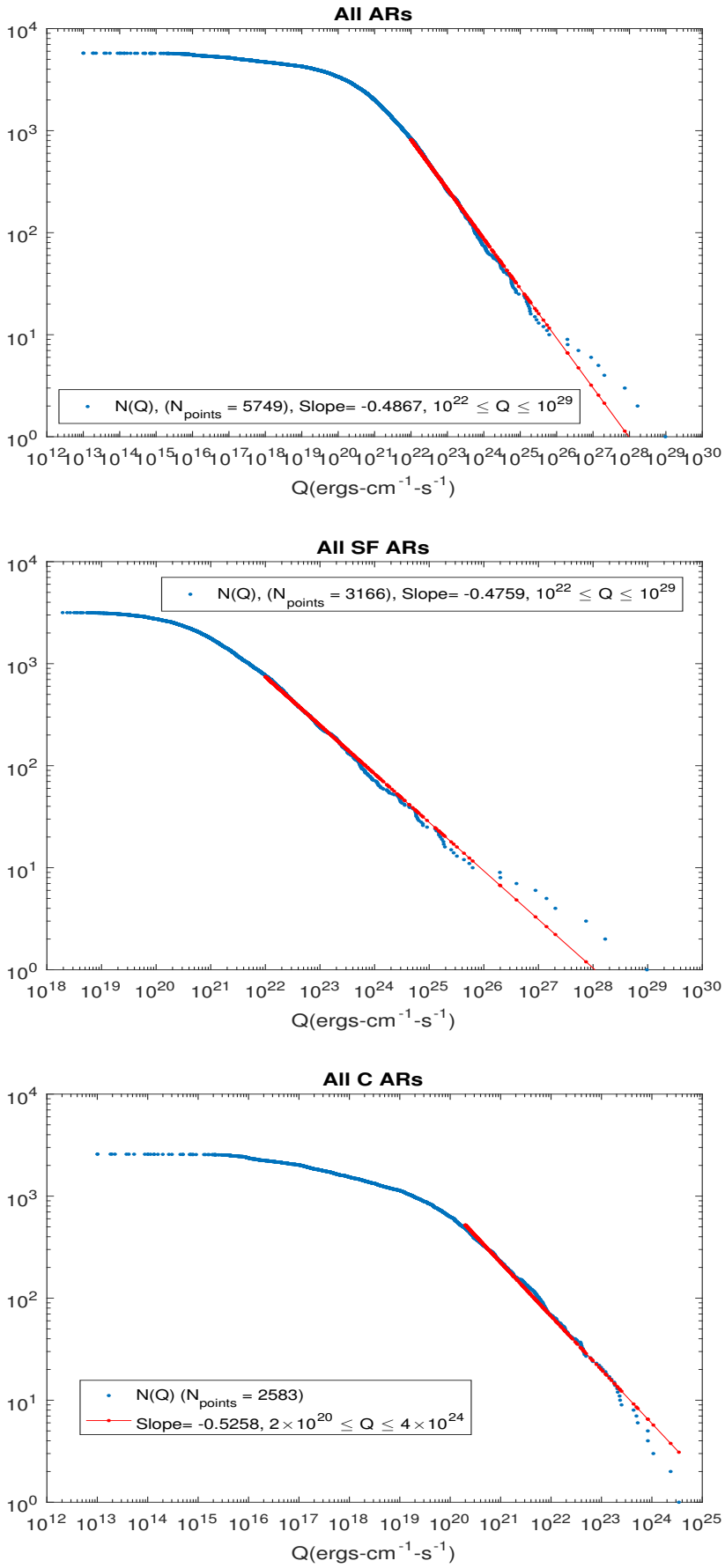

Figure 9: CDFs for all ARs, all SF ARs, and all C ARs.

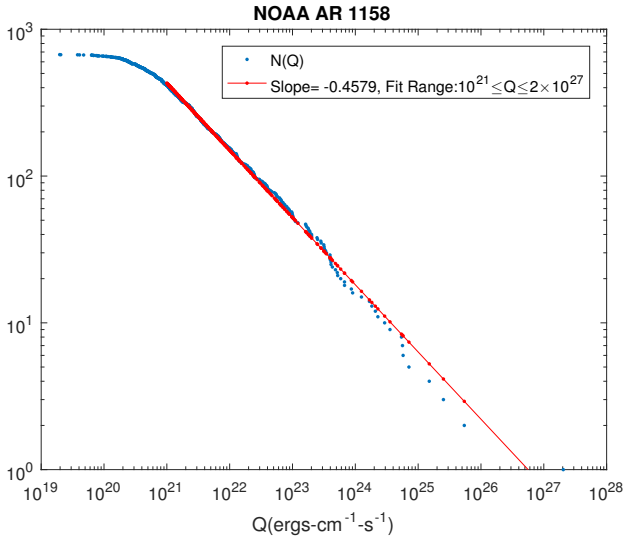

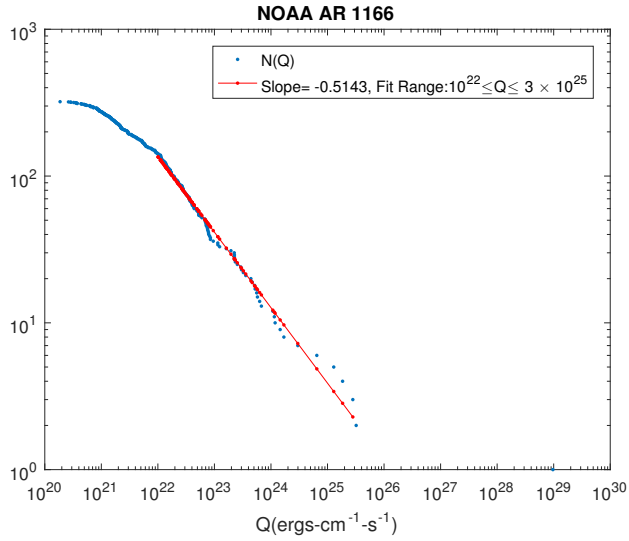

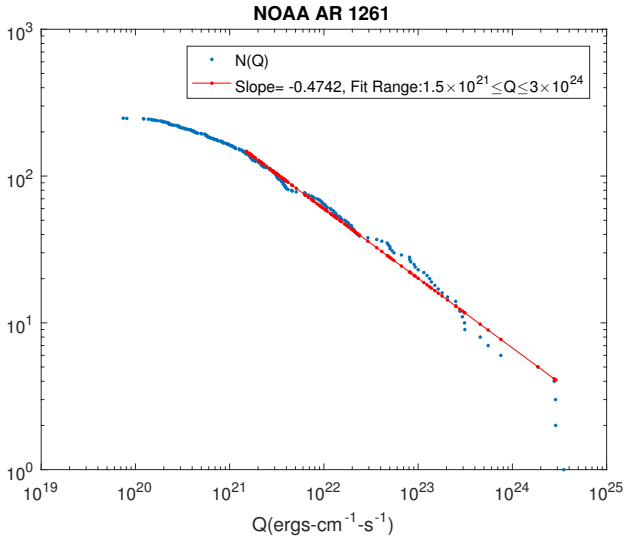

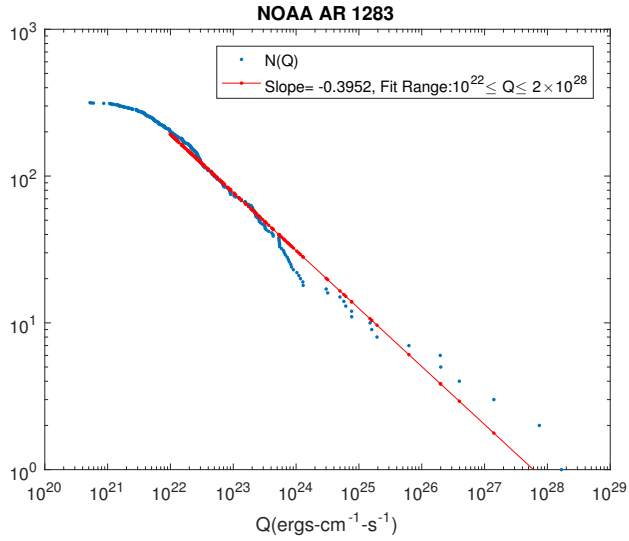

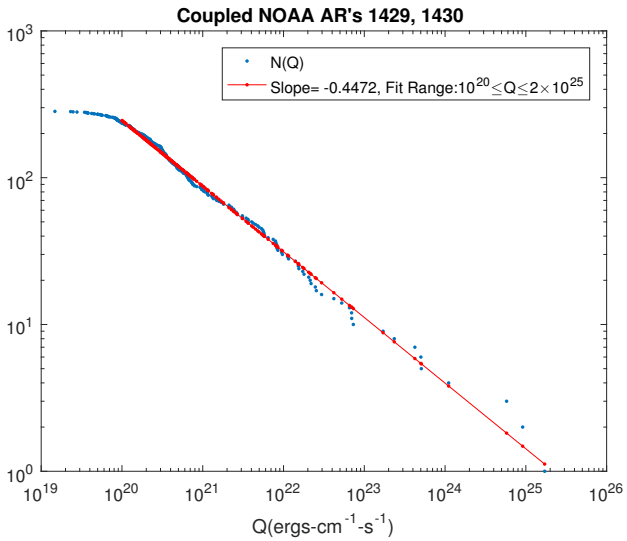

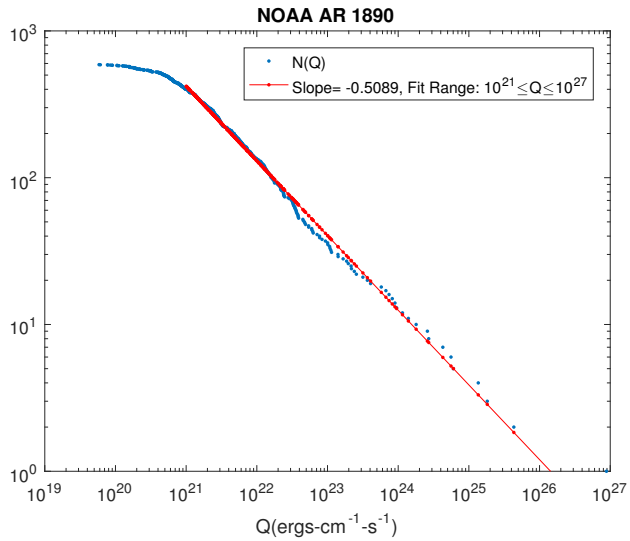

Figure 10: CDFs for SF ARs 1158, 1166, 1261, 1283, 1429/1430 (coupled), and 1890.

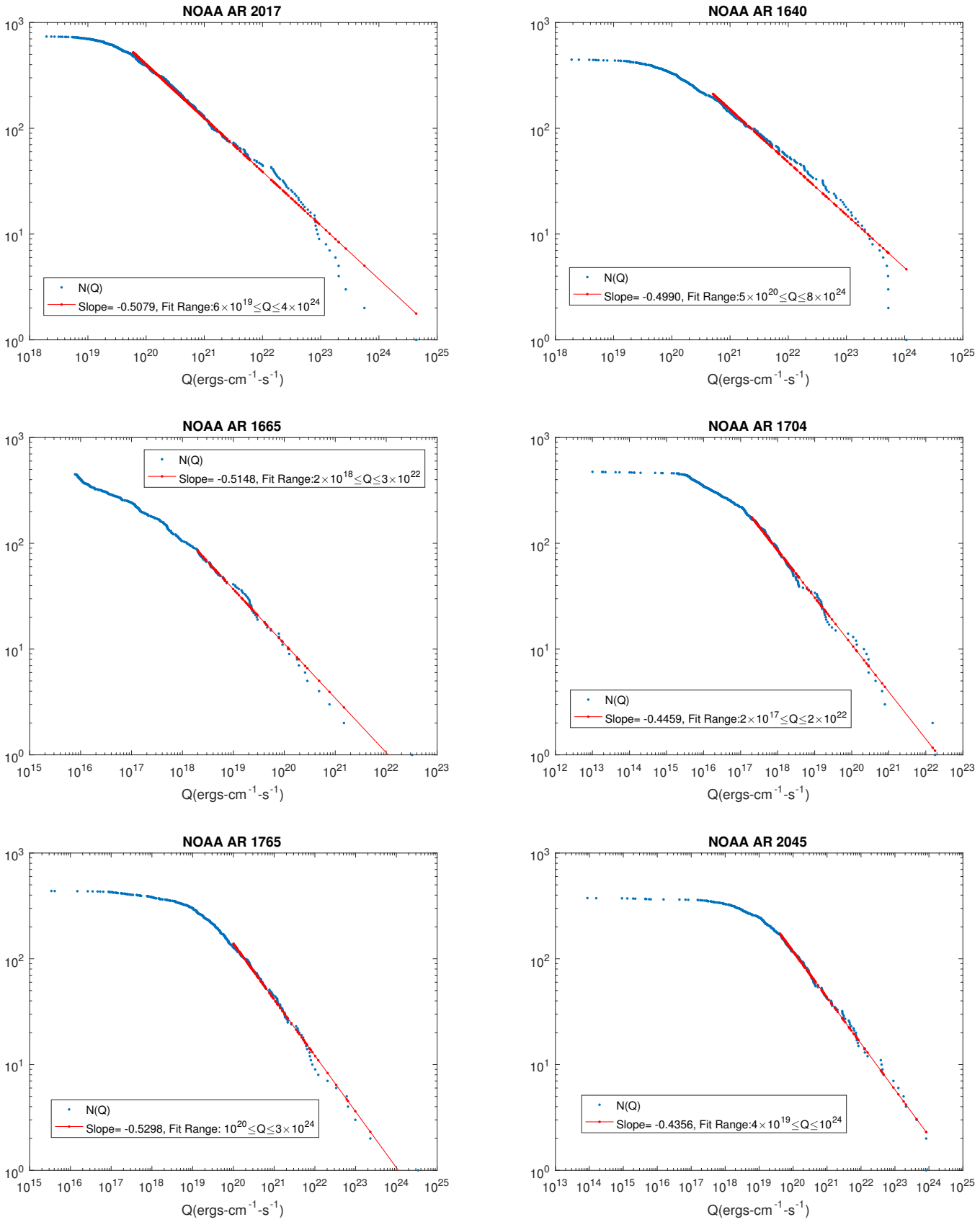

Figure 11: CDFs for SF AR 2017, and C ARs 1640, 1665, 1704, 1765, and 2045.

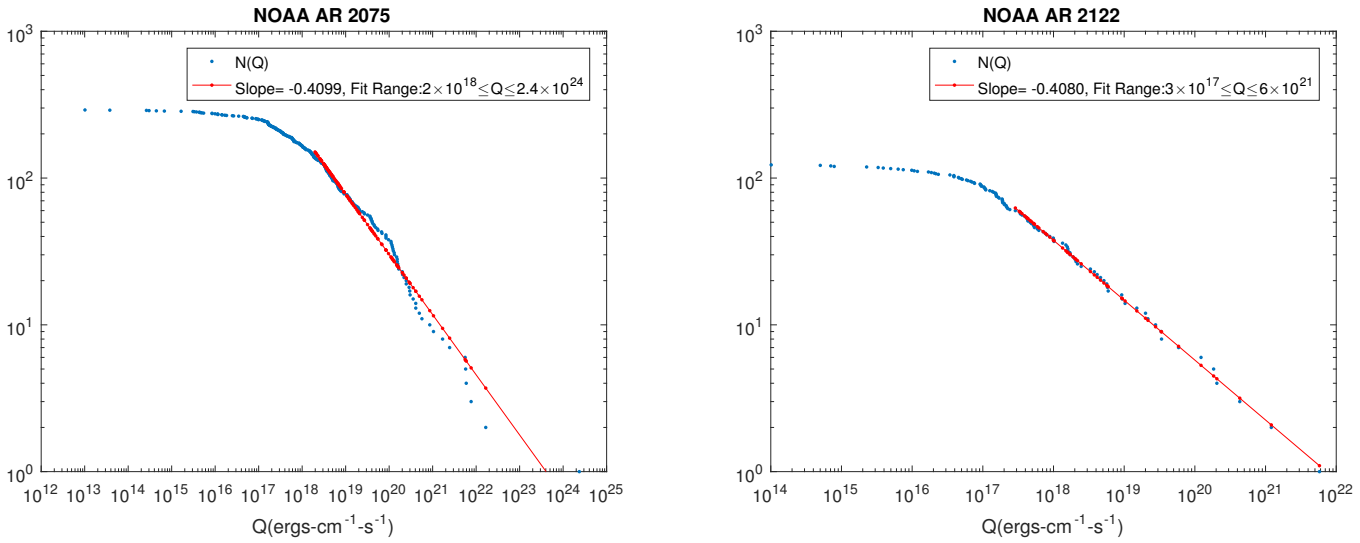

Figure 12: CDFs for CARs 2075 and 2122.

8. Power Spectra and Spectrograms of the Time Series of Q

- **The following figures show the power spectrum and spectrogram for each AR.**
- **Power Spectra: For 6 ARs the spectra show decreases in power by orders of magnitude at certain frequencies. For 3 ARs the spectra clearly show periodic oscillations in frequency.**
- **Spectrograms (Time-Frequency plots): In almost all cases the spectrograms show periodic intensity variations by orders of magnitude with respect to frequency at certain times.**
- **The origin of this non-random structure in the power spectra and spectrograms remains to be explained.**

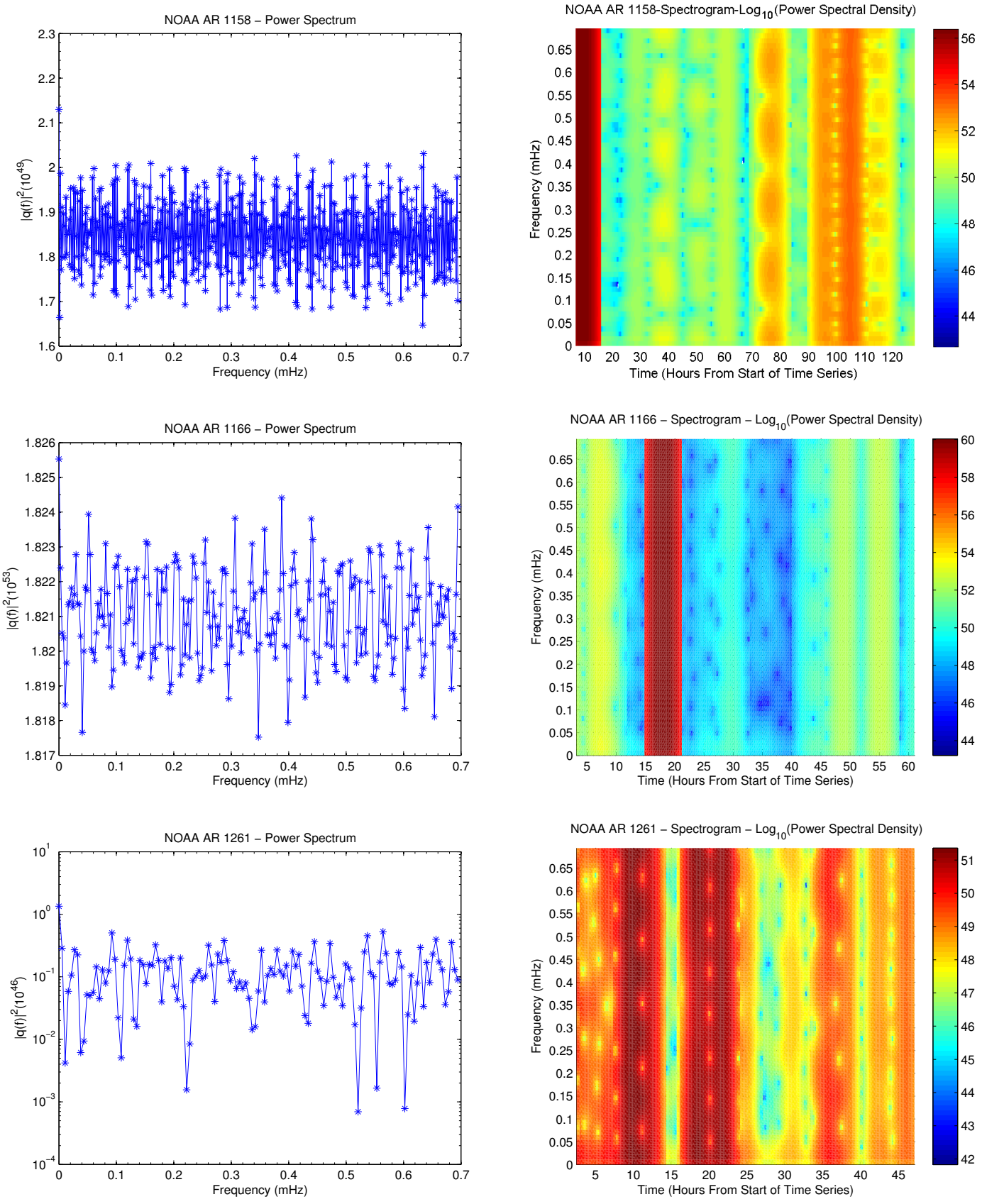

Figure 13: Power Spectra and Spectrograms for SF ARs 1158, 1166, 1261.
(A period of one hour corresponds to a frequency of 0.28 mHz.)

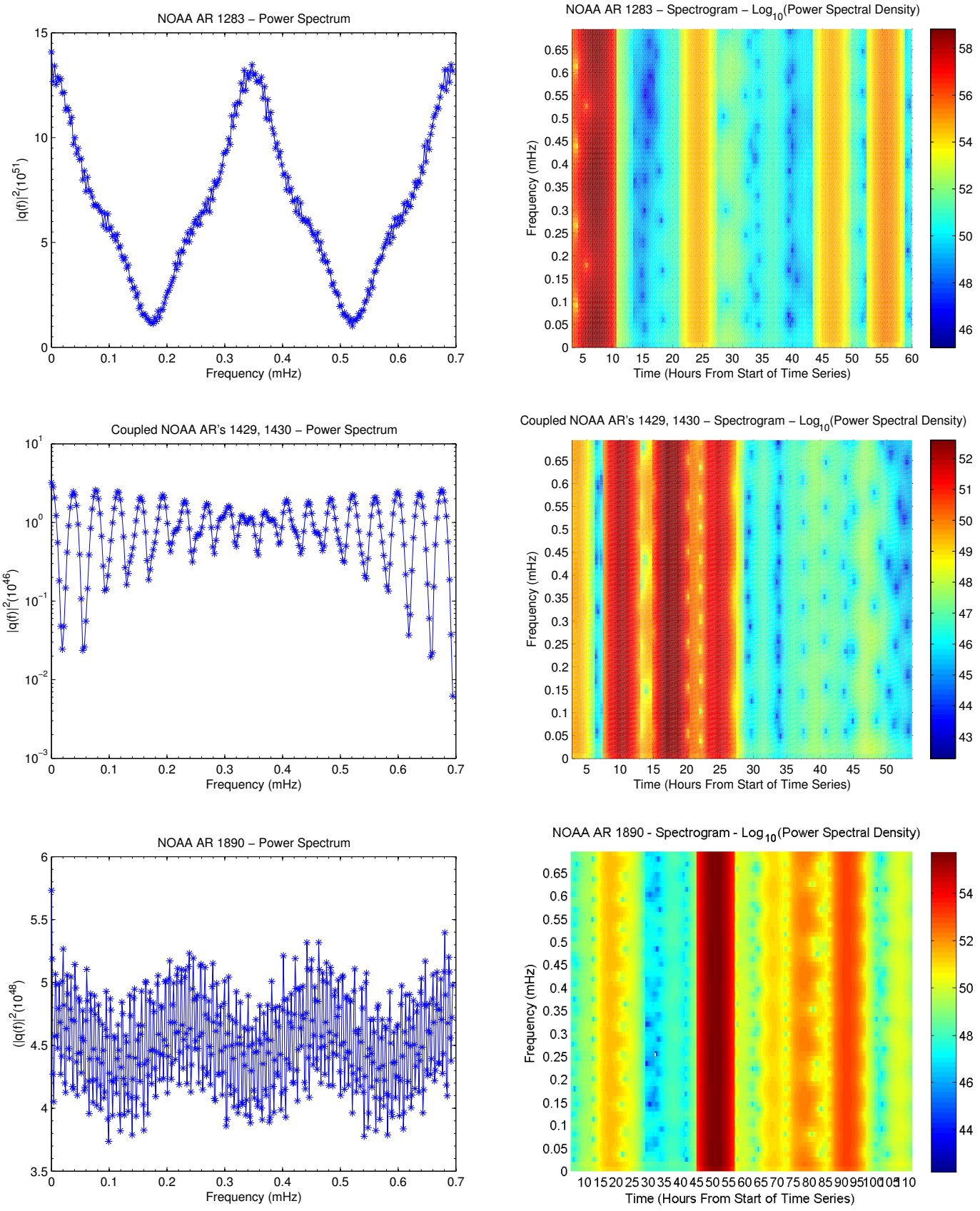

Figure 14: Power Spectra and Spectrograms for SF ARs 1158, 1429/1430, 1890.

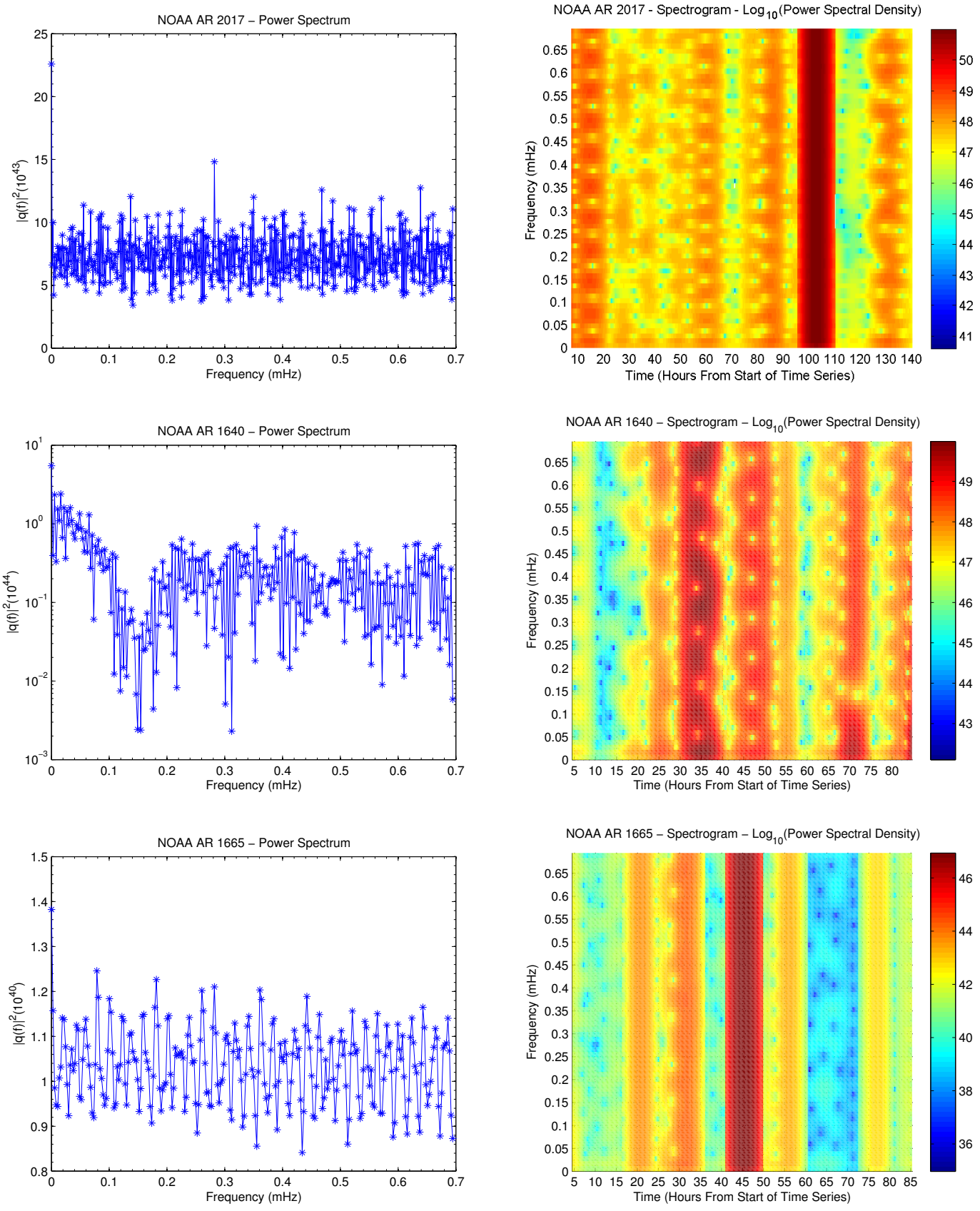

Figure 15: Power Spectra and Spectrograms for SF AR 2017, and C ARs 1640, 1665.

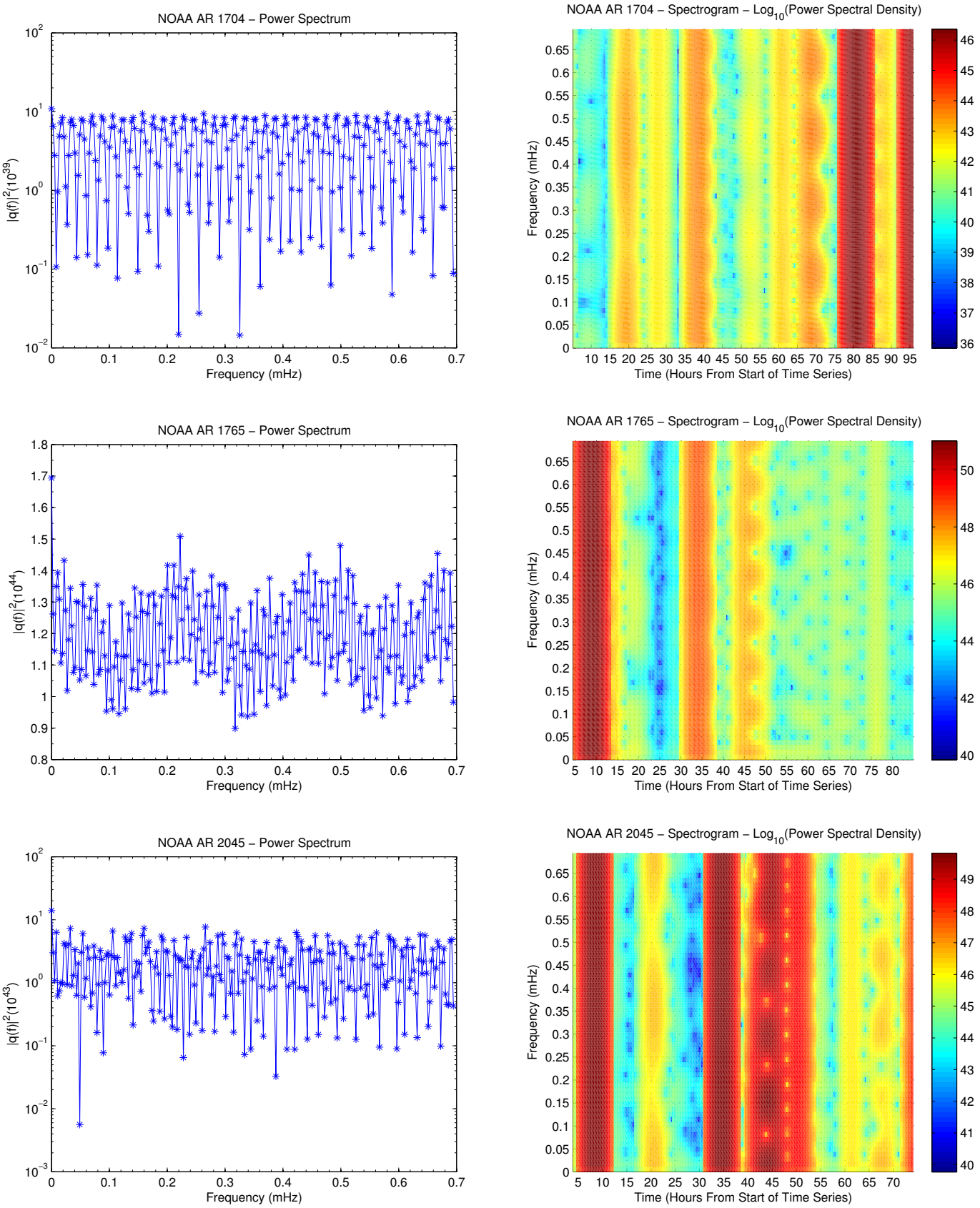

Figure 16: Power Spectrua and Spectrograms for C ARs 1704, 1765, 2045.

9. Conclusions

- **Photospheric current spikes, and associated resistive heating spikes, several orders of magnitude above background values occur on granulation space and time scales in NLRs of ARs.**
- **The largest spikes occur in NLRs that exhibit M/X flares. They are highly non-force-free.**
- **It is plausible these events are correlated with M/X flares, preceding them by several hours to several days. But the sample size of 14 ARs is too small to determine if a correlation exists. Analysis of more and longer time series is needed to determine this.**
- **The CDFs of the time series of Q for all 14 ARs obey a scale invariant power law distribution essentially identical to that observed for the total energy of solar flares. This suggests a strong similarity between the mechanism of the granulation scale *photospheric* heating events found here, and the mechanism of flare energy release, which is a *coronal* phenomenon on scales 10 - 100 times larger.**
- **The spikes may be driven by reconnection in horizontal, granulation scale current sheets, and be signatures of photospheric or lower chromospheric bombs.**
- **Future Work:**
  (1) Analyze more time series to determine if there is a correlation between the times of the largest spikes in Q, and the times of subsequent M/X flares.
  (2) Determine the physical basis of the structure in the power spectra, spectrograms, and CDFs of the time series of Q.